JOURNAL OF CATALYSIS **178,** 198–206 (1998)
ARTICLE NO. CA982144

Synthesis of Short Fibrous Boehmite Suitable for Thermally Stabilized Transition Aluminas Formation

Kamal M. S. Khalil

Chemistry Department, Faculty of Science, South Valley University, Sohag 82524, Egypt

Received December 29, 1997; revised April 20, 1998; accepted April 28, 1998

Transmission electron microscopy showed that xerogel of long and short fibrous boehmite samples, AlO(OH), were respectively produced via hydrolysis of aluminium alkoxide at slow and high stirring rates. Thermogravimetry, differential scanning calorimetry, and X-ray diffractometry, showed the two xerogels to produce similar calcination products, at 400°C and up to 1000°C, for the chemical and phase composition of the material bulk. In contrast, nitrogen adsorption measurement revealed different surface textural consequences of the boehmite fiber length. It has been concluded that the short fiber boehmite produces on calcination aluminas that are more resistant to particle sintering (thermally stabilized) than the long fiber boehmite.

Key Words: **alkoxide derived boehmite; stabilized alumina; high surface area alumina.**

1. INTRODUCTION

Surface texture and thermal stability largely determine the performance of catalytic aluminas (1). In fact, these properties are influenced strongly by the preparation method applied and depend on the major phase present (1–5). Alkoxide derived fibrous boehmite is an important precursor for preparation of high surface area single (6–10) and mixed aluminum oxide (11–13). Alkoxide-derived boehmite is normally produced by the Yolads process (14, 15). The process involves hydrolysis of aluminum iso-propoxide (or sec-butoxide) in excess of water, followed by peptization via acid addition. Aging over a period of ~24 h at 80°C yields the production of boehmite, whereas aging at room temperature results in bayerite, $Al(OH)_3$. When porous texture and high surface areas are preferred, it is necessary to maintain the textural properties of the wet-hydrolysed gel by adopting the appropriate drying method (16).

The structure of the hydrolyzed gel largely controls the thermal properties of the produced alumina. An alkoxide-derived alumina calcined at 500°C (and still amorphous) exhibits a surface area as 600 m^2/g (17). However, this alumina calcination product completely transfers to α-alumina of very low surface area (17) at a temperature as low as 800°C. This poor structural stability was attributed to the amorphous nature of the parent alumina. Murrell and Tauster (18) concluded that an alumina sol of a critical size range (not less than ca 20 nm) can be transformed into the final alumina structure without significant aggregation, which otherwise (for smaller particles) produce a dense alumina structure of lower surface area. Moreover, the phase transition of γ-alumina into α-alumina (at ca 1000°C), which leads to a drastic decrease in specific surface area, may be slowed down by adding small amounts of a different oxide (7, 8). However, catalysis on these modified aluminas might be different from that on pure aluminas. Thus, thermal stabilization of γ-alumina is welcomed if achieved using pure boehmite (7).

Different methods have been reported for the preparation of thermally stable ultra pure alumina derived from aluminum *tri*-isopropoxide. These include, fume pyrolysis of fibrous boehmite sol (7), where the achieved stability was ascribed to suppression of the rate of phase transformation to α-alumina caused by the fact that alumina particles were of crude structures assembled from fibrils. Another attempt has been done by heat treatment of hydrolyzed Aluminum iso-propoxide sol of fibrous particles mixed with carbon matrix (saccharose) (8). Further improvement of the thermal, texture, and structural properties of alumina may be achieved via a super critical drying method (19–21). Decreasing the zeta-potential of the boehmite particles during aging gives rise to better structural stability, too (22). It has been reported (23) that high surface area alumina may be synthesized by applying an inert solvent, polar super critical fluids, and large dilution of aluminum alkoxide.

The above survey highlights that short fibrous boehmite of a certain range of size is the base point for stabilized texture formation of alumina. Our previous investigations (24–25) have indicated that fibrous boehmite can be produced through a single-stage preparation method. The method utilizes a 1:1 water/alkoxy ratio in a nonpolar solvent. Thus it is different from the Yoldas method which utilizes high water/alkoxy ratio in polar solvents. The present work describes the controlling of the size of the produced fibrous boehmite. Examining structural, textural, and thermal stability of the produced xerogel in

0021-9517/98 $25.00

relation to the preparation conditions. These properties were determined by X-ray powder diffractometry (XRD), transmission electron microscopy (TEM), thermogravimetry (TG), Differential scanning calorimetery (DSC), and N_2 adsorption volumetery.

2. EXPERIMENTAL METHODS

2.1. Boehmite Preparation

Two boehmite xerogel samples were prepared using the following procedure. Aluminum *tri*-isopropoxide (99.99%, Aldrich) 0.05 molar solution in *n*-heptane was hydrolyzed by a dropwise addition of a calculated amount of water to furnish the 1 : 1 water/alkoxy ratio. The solution was stirred magnetically at 100 rpm (slow-stirred sample), or at 800 rpm (fast-stirred sample). Stirring was allowed to continue for 30 min in each case; then the obtained gel was allowed to stand for 3 days without any further stirring. Subsequently, the gel was filtered off from its solution and allowed to dry at room temperature for an overnight period and then at 60°C for 24 h. To examine the surface and the texture for the two xerogels, portions of the xerogels were calcined in a Muffel furnace for 3 h at 400, 800, and 1000°C. An additional calcination for 10 h at 1000°C for the two xerogels was made. Moreover, a group of materials (for the two xerogels) were calcined at 400–1000°C for 30 h and examined by XRD (see XRD results below).

2.2. Thermal Analysis

A thermal analyst 2000 TA instrument controlling a 2050 thermogravimetric analyzer and a 2010 differential scanning calorimeter was used. For thermogravimetry (TG) a platinum sample boat was used with the sample size being 10.0 ± 0.1 mg. The heating rate was 5°C/min in flow of nitrogen gas at the flow rate of 30 ml/min. Transition temperature analysis was carried out for each region in each TG curve using the TGA 5.1 software of the instrument indicated.

For differential scanning calorimetry (DSC) measurement, aluminum sample pans were used with the sample size 3.0 ± 0.1 mg. Each sample pan was covered with a lid to improve sample-to-pan contact, but without crimping of the pan to allow volatile materials to skip out. Measurement was carried out against an empty covered and crimped aluminum pan as a reference, following cell constant determination and temperature calibration. The heating rate was 5°C/min. Transition temperature analysis was carried out for each region in each DSC curve using the DSC 4.0 software of the instrument indicated.

2.3. X-Ray Powder Diffractometry (XRD)

XRD powder diffractograms were recorded for the test samples by means of a model JSX-60 PA Jeol diffractometer, equipped with a Ni-filtered CuK_α radiation. For identification purposes diffraction patterns thus obtained were matched with JCPDS standards (26).

2.4. Transmission Electron Microscopy (TEM)

TEM micrographs were obtained, using a model JEM-1010 Jeol microscope (Japan). Test samples were prepared by ultrasonic dispersion of the solid in isopropanol. A drop of the resulting suspension was doped onto a carbon-coated grid and allowed to dry at 60°C. A number of grids were prepared for each sample by this method and investigated by TEM at 100 kV. The 400°C calcination products were selected as representative for the morphology of the precursor materials. This was because low calcination temperature samples are less stable under the electron beam of the microscope and take advantage of the topotactic nature of the boehmite fiber.

2.5. Nitrogen Gas Adsorption

N_2 gas adsorption/desorption isotherms were measured at −196°C using a model ASAP 2010 (Micromertics Instrument Corporation, USA). Test samples were thoroughly outgassed for 2 h at 250°C. The specific surface area, S_{BET}, was calculated applying the BET equation (27). Porosity distribution was generated by DFT plus V1.00 (2010) software of the instrument indicated implementing the classical Kelvin equation, slit like pore shape, and Halsey thickness curve (28).

3. RESULTS

3.1. Characteristics of the Dry Hydrolysis Products

Figure 1 shows the XRD patterns of the slow and fast stirred dry hydrolysis products (xerogels). Clearly the two patterns are largely similar, in indexing aluminum

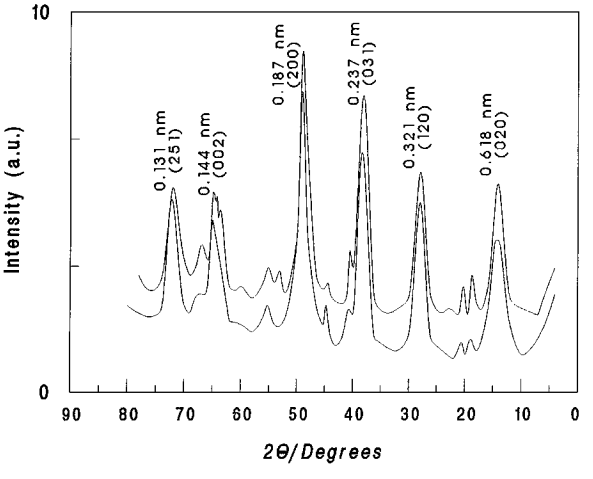

FIG. 1. XRD patterns obtained for the slow- and the fast-stirred xerogels.

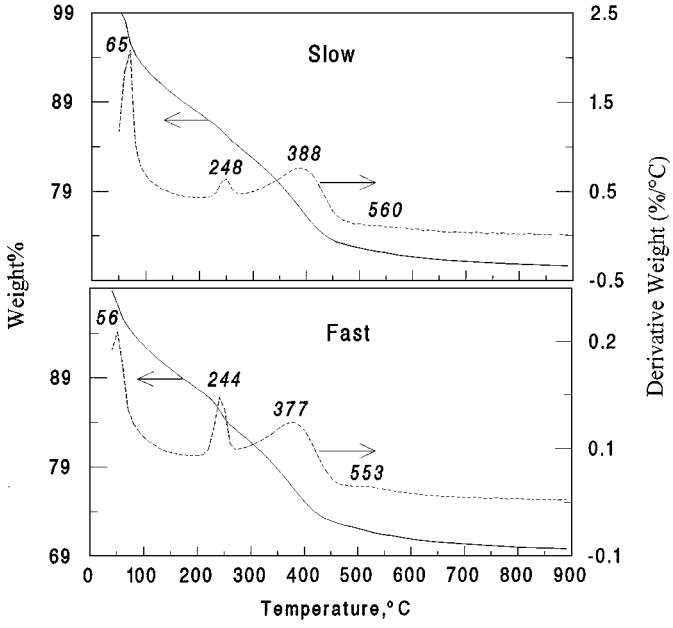

FIG. 2. TG and DTG curves recorded for the slow- and the fast-stirred xerogels.

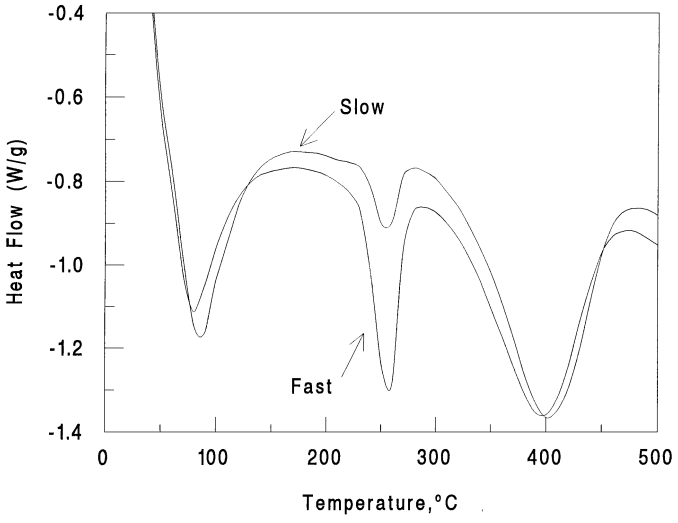

FIG. 3. DSC curves recorded for the slow- and the fast-stirred xerogels.

oxyhydroxide, *boehmite*. TG curves recorded at 5°C/min for the two xerogels are shown in Fig. 2, along with their DTG curves. The figure shows that dehydration occurs gradually, with no sign of weight stable steps. However, four weight loss regions may be characterized for each sample. These weight loss regions are indicated by "start" and "stop" temperatures in Table 1. Results of the transition temperature analysis for each start–stop temperature region as "onset, maximum, and end" of transition step are cited in Table 1, along respective chemical formula.

Figure 3 shows the DSC curves recorded at 30–500°C, and 5°C/min for the two xerogels. Three endothermic peaks are observed for each sample. The onset and maximum temperatures for each start–stop region indicated are cited in Table 2, along with the area of each peak measured in J/g.

TEM micrographs, shown in Figs. 4a and 4b, indicate the textural differences between the two xerogels. It is obvious that the slow stirring resulted in long (ca 200 nm) fibrous boehmite of crumpled sheet-like morphology (a), whereas the fast stirring resulted in short (ca 50 nm)—relatively—straight ones (b).

3.2. Characteristics of the Xerogels Calcination Products

XRD patterns were recorded for the 400, 800, and 1000°C (3 h) calcination products of the two xerogels. The patterns reveal that the calcination products were amorphous. Nevertheless, the patterns recorded for the 800 and 1000°C calcination products (of the two xerogels) show very small peaks which could be related to the main *d*-spacing of γ- and θ-alumina, respectively. To explore the ultimate change that would occur upon prolonged calcination (i.e., structural stability) of the above materials. Portions of the two xerogels were calcined for 30 h at 400–1000°C.

TABLE 1

TG Results for the Two Xerogels as the Onset, Maximum, End, Loss Percentage for Each Start–Stop Range Indicated for the Different Dehydration Steps

Precursor dehydration step		Start (°C)	Onset (°C)	Max (°C)	End (°C)	Stop (°C)	W (%)	Formula[a]
Slow	I	44	62	65	77	181	88.47	$AlO(OH)\cdot 0.78H_2O$
	II	181	235	248	257	277	83.74	$AlO(OH)\cdot 0.58H_2O$
	III	277	343	388	434	496	72.65	$1/2Al_2O_3\cdot 0.26H_2O$
	IV	496	541	560	660	890	70.58	$1/2Al_2O_3\cdot 0.09H_2O$
Fast	I	31	32	56	77	191	87.97	$AlO(OH)\cdot 0.75H_2O$
	II	192	231	244	252	280	82.61	$AlO(OH)\cdot 0.37H_2O$
	III	280	335	377	423	480	72.30	$1/2Al_2O_3\cdot 0.23H_2O$
	IV	480	534	553	651	893	69.71	$1/2Al_2O_3\cdot 0.02H_2O$

[a] H_2O values were calculated based on considering that the weight recorded (69.46%) for the fast-stirred xerogel at 1000°C as $Al_2O_3\cdot 0.00H_2O$.

Figure 5 shows XRD patterns for the 30-h calcination products at 600, 800, and 1000°C for the slow stirred xerogel. The patterns are rather similar to those obtained for the long fibers. Indexing of the patterns (26) reveals that the calcination products at 400°C, of the two xerogels, were completely amorphous (not shown in Fig. 5). Just slight crystallinity into gamma alumina commenced to appear after calcination at 600°C and developed considerably at 800°C. The 1000°C calcination resulted in a phase transition into weakly crystalline θ-alumina.

Nitrogen gas adsorption was measured at liquid nitrogen temperature on the 400, 800, 1000°C (3 h), and 1000°C (10 h) calcination products of the two xerogels.

The N_2 adsorption/desorption isotherms for the 3-h calcination products for the slow- and fast-stirred xerogels are shown in Figs. 6 and 7, respectively. Isotherms of the 400°C/3 h calcination (curves indicated "a" on the corresponding figures) are of type IV of isotherm indicating mesoporous surfaces (29). They exhibit type H3 hysteresis loops, which are normally observed for aggregates of plate-like particles giving rise to slit-shaped pores (29). Isotherms for the 800 and 1000°C/3 h calcination products assume similar type and hysteresis loops. The 1000°C/10 h calcination product of the slow stirred xerogel (isotherm "d" on Fig. 6) indicate a change in the isotherm type, namely from type IV to type I, and the complete disappearance of the hysteresis loop. A slight change in the isotherm type (into type I) is shown for the fast-stirred materials (isotherm "d" on Fig. 7), and the hysteresis loop still some what recognizable. These results may imply that the slow-stirred material is more sintered at 1000°C/10 h than the fast one.

The specific Surface area, S_{BET}, and c_{BET} values are shown in Table 3. Figure 8 shows the change of S_{BET} as a function of calcination. The results indicate that the 400°C/3 h calcination products of the slow stirred material has got higher surface area than the corresponding calcination products of the fast-stirred material. However, the latter maintains higher surface area upon calcination at higher temperatures.

TABLE 2

DSC Results for the Two Xerogels as the Onset, Maximum, and Peak Area (ΔH) for Each Start–Stop Range Indicated for the Different Dehydration Steps

Precursor step		Start (°C)	Onset (°C)	Max (°C)	Stop (°C)	ΔH (J/g)
Slow	I	50	51	85	160	101.0
	II	194	234	254	272	13.5
	III	279	325	402	472	170.1
Fast	I	52	53	81	160	67.5
	II	194	238	256	283	48.8
	III	295	319	394	467	143.7

TABLE 3

Surface Area, c_{BET}, and Volume in Pores of the Materials Calcined at Different Temperatures

Calcination temp. (°C)	Surface area (m^2/g)		c_{BET}		Volume in pores (cm^3/g)			
					<1.80 nm		>200 nm	
	Slow	Fast	Slow	Fast	Slow	Fast	Slow	Fast
400/3 h	389	376	218	311	0.107	0.111	0.343	0.31
800/3 h	240	257	197	121	0.073	0.072	0.186	0.21
1000/3 h	182	227	94	141	0.052	0.068	0.145	0.17
1000/10 h	139	171	88	113	0.047	0.057	0.088	0.11

Figures 9 and 10 show the pore volume distribution (PVD) curves for the different calcination products of the slow and the fast stirred xerogels, respectively. PVD for the 400°C/3 h calcinations of the slow and the fast-stirred materials are shifted toward the micropore limit and smoothly distributed throughout the mesopore range (2–50 nm). Maxima appear near 2, 5, and 15 nm for the slow, and near 2, 7, and 30 nm for the fast stirred material. PVD for the higher calcinations are smoother for the slow-stirred material. Similar PVD was obtained for the fast-stirred material; nevertheless, a new maximum emerged around 7 nm for the 1000°C/3 h and 1000°C/10 h calcination products. Generally speaking, porosity of any slow-stirred materials is less than the corresponding fast-stirred one, as the area below the distribution curves indicated.

Finally, N_2 volume (ccm/g) in pores <1.8 nm (micropores) and in pores >200 nm for the different calcinations were calculated (see Table 3) and represented in Fig. 11. The figure indicates that reasonably high porosity (either <1.8 or >200 nm) was preserved at high calcinations, especially for the group prepared from the fast-stirred material.

4. DISCUSSION

The results presented above may be outlined as follows:

1. Boehmite xerogels were produced at room temperature, as evidenced by XRD results. Slow-stirring rate resulted in the formation of long fibrous (ca 200 nm long) boehmite, whereas fast-stirring rate resulted in the formation of short fibrous (ca 50 nm long) boehmite.

2. Calcination products of the long and the short fibrous boehmite exhibited good structural and textural stability. However, the short fibrous boehmite phase stability leads to better textural stability upon calcination at higher temperatures. Weakly crystalline γ-alumina commenced to appear at 600°C and developed at 800°C; phase transition into weakly crystalline θ-alumina occurs at 1000°C.

Thus, the following discussion will compare the present results in relations to those of other published work.

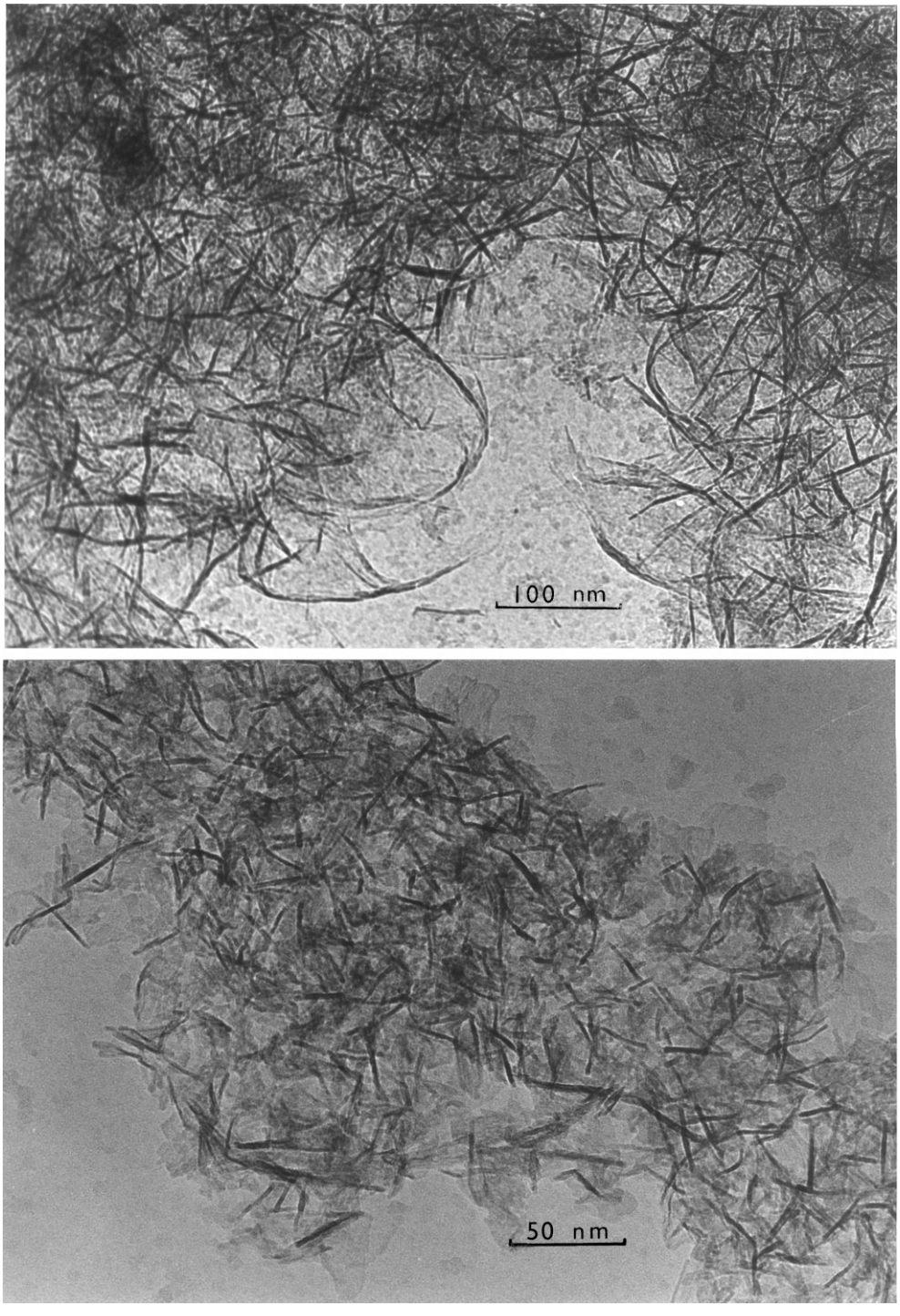

FIG. 4. TEM micrographs for the slow (top) and the fast (bottom) stirred xerogels, indicating long (ca 200 nm) and short (ca 50 nm) fibrous morphology.

4.1. The Formation of Fibrous Boehmite at Room Temperature

According to Yoldas process (14, 15), which utilizes high water/alkoxy ratio, boehmite, AlO(OH), can only be produced by aging at 80°C. But, due to the high water/alkoxy ratio employed, there appears to be little evidence that under this aggressive hydrolysis conditions the oligomeric structure of $Al(OR)_3$ precursor is maintained. Thus it is not surprising that many similarities do exist between this

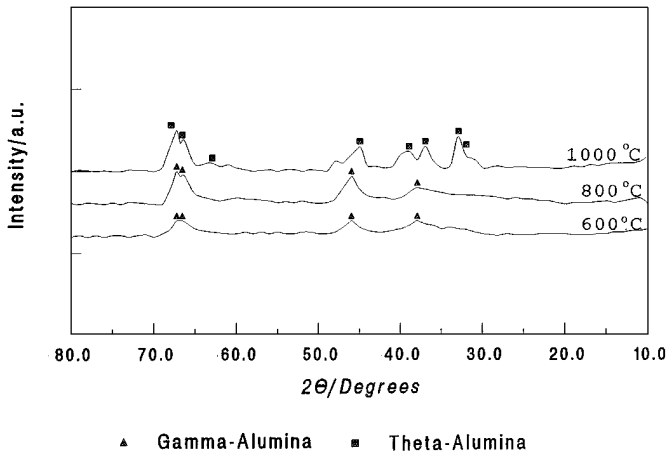

FIG. 5. XRD patterns of the short fibrous boehmite calcined for 30 h at the indicated temperatures.

route and the aqueous one (from inorganic precursors) (30).

Assih *et al.* (31) postulated that a boehmite-like structure forms during Yoldas sol concentration. Furthermore, they suggested that under these conditions hydrolysis may occur without destroying the original oligomeric structure. Hydrolysis at the interface between a limited amount of water/nonaqueous aluminum sol media (the present conditions) led to partial hydrolysis of the aluminum *tri*-isopropxide. The polar nature of the partially hydrolyzed species will force them to accumulate and condense at the interface. It is important that under these conditions hydrolysis may occur without destroying the original oligomeric structure due to the concentration of the hydrolyzed species at or in the small droplets of water slowly stirred in the nonpolar media. Thus, condensation between partially hydrolyzed species retaining their polymeric structure should lead to fibrils structure. Increasing the stirring rate would lead to further dispersion of water droplets, resulting in smaller ones containing, of course, less content of the precursor material. Thus, finer particles will form upon condensation. Thus despite the oligomeric structure which could be maintained (i.e., boehmite is produced), there

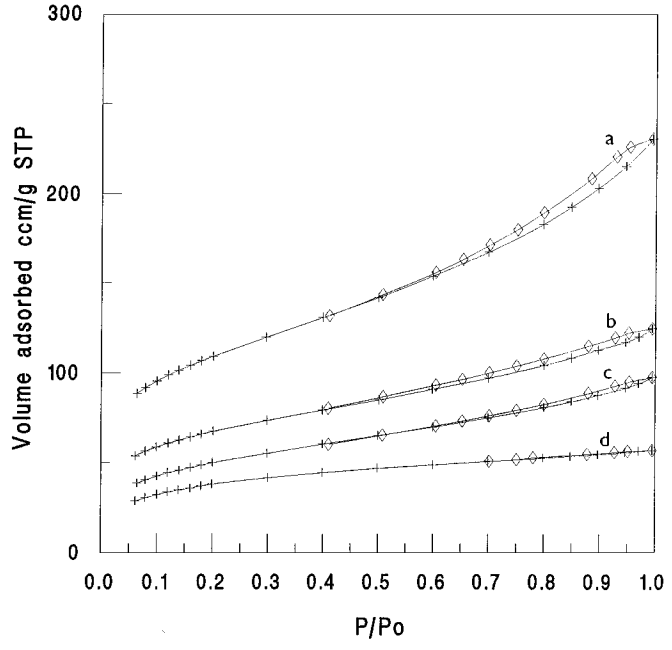

FIG. 6. N_2 adsorption/desorption isotherms of alumina obtained by the slow stirred xerogel calcination at the 400°C/3 h (a), 800°C/3 h (b), 1000°C/3 h (c), and 1000°C/10 h (d).

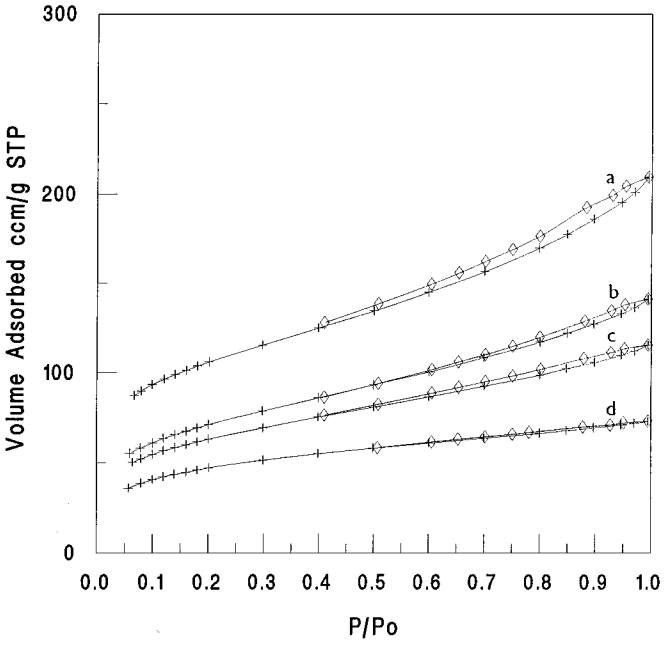

FIG. 7. N_2 adsorption/desorption isotherms of alumina obtained by the fast stirred xerogel calcination at the 400°C/3 h (a), 800°C/3 h (b), 1000°C/3 h (c), and 1000°C/10 h (d).

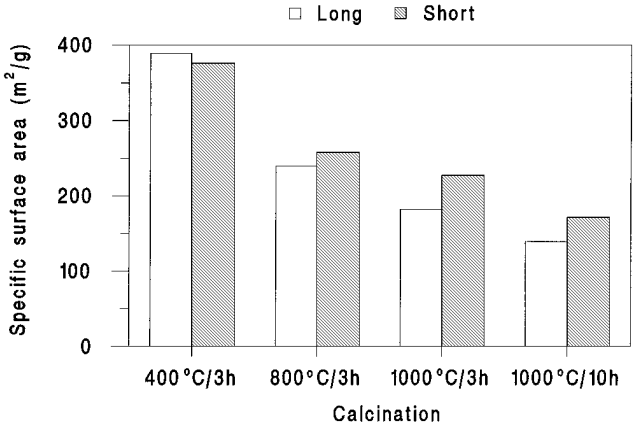

FIG. 8. Specific surface area of the calcination products of the slow- and the fast-stirred xerogels as a function of calcination.

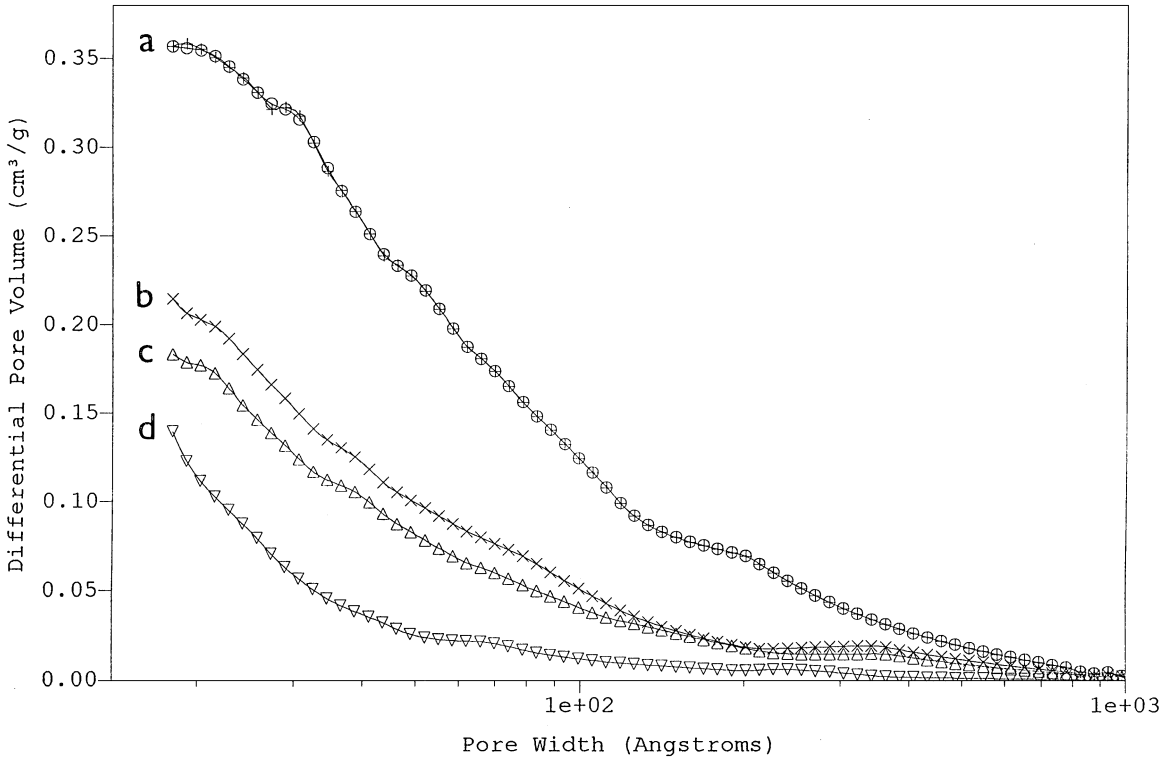

FIG. 9. Pore size distribution of alumina obtained with the slow-stirred xerogels calcination at the 400°C/3 h (a), 800°C/3 h (b), 1000°C/3 h (c), and 1000°C/10 h (d).

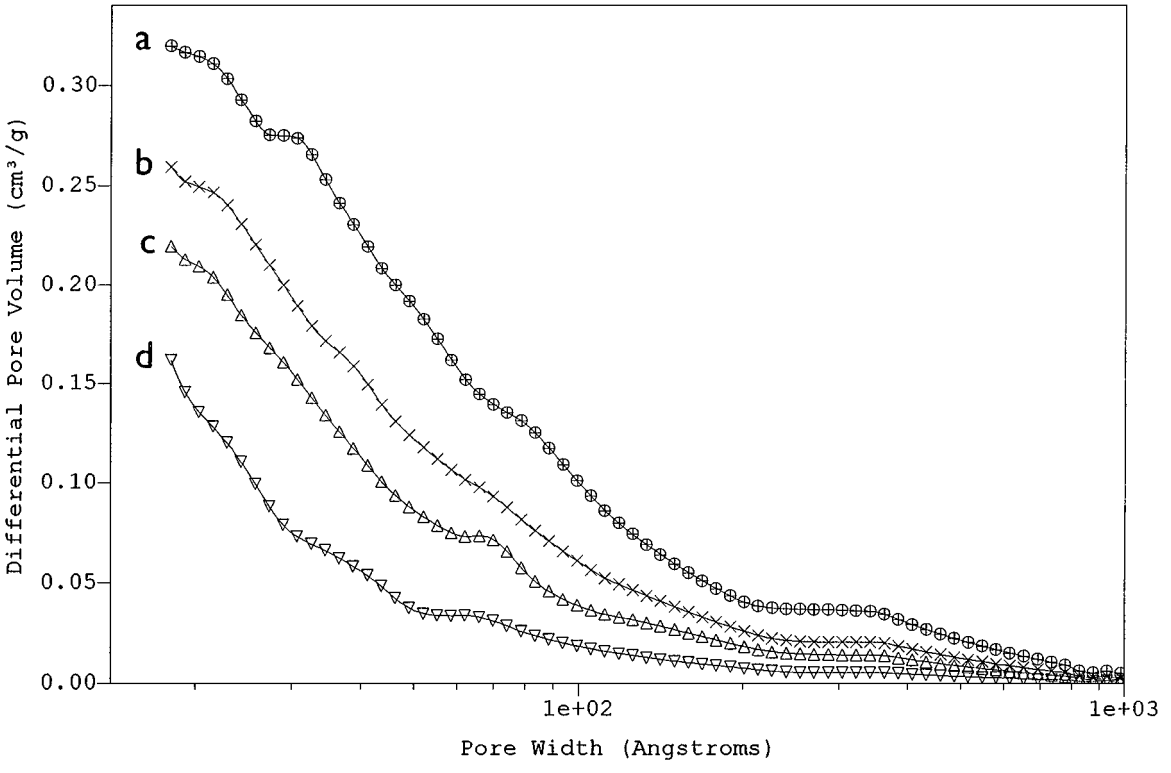

FIG. 10. Pore size distribution of alumina obtained with the fast-stirred xerogels calcination at the 400°C/3 h (a), 800°C/3 h (b), 1000°C/3 h (c), and 1000°C/10 h (d).

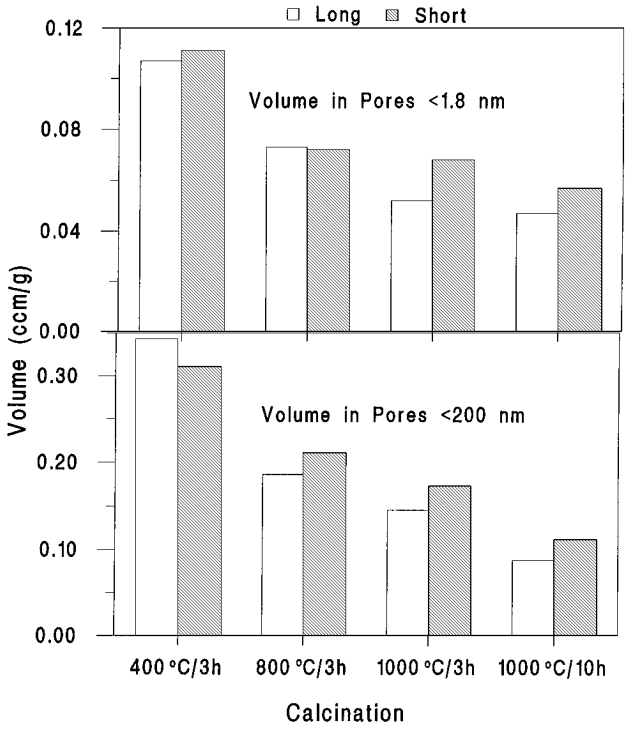

FIG. 11. Volume in pores <1.8 nm and >200 nm for the calcined products of the slow- and the fast-stirred xerogels as a function of calcination.

is a slight chance for the formation of long fibrous structures.

Furthermore, a slow stirring rate slows down the partial hydrolysis process, allowing for the condensation reaction to take place. In contrast, fast stirring may result in fast initial hydrolysis, giving rise to more nuclei and consequently smaller particles than the previous case.

Evidence for the above mechanism, which relates the morphology difference to the initial droplet size, can be drawn from the fact that the hydrolyzed gel was allowed to age for three days before drying. Even so, two distinctly different textures were obtained. Thus, the texture is determined essentially by the droplet size (which is related to the stirring rate), and long aging could not cause the conversion of the small particles to larger fibers.

4.2. Thermal Stability of the Short Fibrous Boehmite

Results showed that the fibrous size of both xerogels exceeds the critical limit suggested by Murrell and Tauster (18), which promises the formation of stabilized alumina. The dried short and long fibrous boehmite gels exhibit weight loss over the range of the dehydration stages I, II, and III (room, ~400°C) due to loss of physically adsorbed, structural, and intercalated water (32). Thus they are gradually transformed into γ-alumina, in a topotactic transformation that is accomplished by internal condensation of protons and hydroxyls between boehmite layers to remove half the oxygen from the layers, cause the collapse and rearrangement of oxygen into cubic close-packing (33).

In lights of the XRD results obtained for both xerogels and their calcination products for a period as long as 30 h, the following structural transformation route may be assign to occur as a function of temperature:

$$\text{Boehmite} \xrightarrow{400^\circ\text{C}/30\,\text{h}} \text{amorphous } \gamma\text{-alumina} \xrightarrow{800^\circ\text{C}/30\,\text{h}} \text{weakly crystalline } \gamma\text{-alumina} \xrightarrow{1000^\circ\text{C}/30\,\text{h}} \theta\text{-alumina.}$$

In terms of the surface area results the prepared xerogels offer the formation of high surface area transitional aluminas upon calcination. However, the transformation of boehmite to γ-alumina and the subsequent transformation to θ-alumina at 1000°C are accompanied by coarsening of the micro structure. This is evidenced by the decreasing values of S_{BET} and increasing values of the average pore size (34). It has been reported that the $\gamma \rightarrow \delta \rightarrow \theta$-$Al_2O_3$ transformation sequence does not involve loss of water (32). But, the present results reported some weight loss upon heating up to 900°C, however small (see TG, Fig. 1). Moreover, TG results showed that the long fibers preserve more water than the short fibers at the end of each dehydration stage, probably due to the little folding morphology of the former (see TEM micrographs). Pierre and Uhlmann (35) have shown that large folding of a boehmite layers may result in the formation of superamorphous gel (in presence of high amount of water). Folding occurs due to stacking faults and leads to intercalation of water, which causes swelling. However, in the present work where a limited amount of water only was available at the stage of boehmite formation. The observed little folding may lead to a kind of local amorphous surface formation within the folded fibers.

Thus, the present results agree well with the model proposed by Soled (36), who proposed a dynamic change model to describe coalescence of γ-alumina particles. This resulted in a surface area decrease and coarsening of the micro structure (36). The dynamic model implies that during coalesce via $-OH$ groups, a terminal oxide ion is formed and becomes incorporated as the bulk anion bridging the two particles. The question now is why the amount of such a dynamic change is so small for the short fibrous particles, i.e. increasing their thermal stability.

To answer the above question, let us first describe the dehydration process in terms of the phase formed, according to Soled (36), formally and stoichiometrically as:

$$Al_2O_3 \cdot H_2O\ (\text{boehmite}) \rightarrow Al_2O_3 \cdot 1/5H_2O\ (\gamma\text{-alumina}) \rightarrow \alpha\text{-}Al_2O_3$$

and

$$\mathrm{AlO(OH)\ (boehmite)} \rightarrow \mathrm{Al_{2.5}\square_{0.5}O_{3.5}(OH)_{0.5}}\ (\gamma\text{-alumina}) \rightarrow \alpha\text{-}\mathrm{Al_2O_3}.$$

If the hydroxide ions populate only the surface and the oxide ions comprise the bulk of γ-alumina, the fraction of anions on the surface is 1/8 and the rest is in the bulk (36). Thus, one can speculate (for the range of size studied) that anions exist in a smaller concentration on the surface of the short fibers than that on the longer ones, since the surface/mass ratio is larger for the former. Thus, if we consider that surface OH anions are the driving force for the model described. It follows that a weaker driving force for coalescence is present in the case of the short particles than for the long ones, and consequently, slower sintering occurs upon calcinations.

REFERENCES

1. Trimm, D. L., and Stanisluas, A., *Appl. Catal.* **21**, 215 (1986).
2. Nortier, P., Fourre, P., Mohammed Saad, A. B., Saur, O., and Lavalley, J. C., *Appl. Catal.* **61**, 141 (1990).
3. Fukui, T., and Hori, M., *J. Mater. Sci.* **31**, 3245 (1996).
4. Kawamura, K., and Endo, H., *J. Ceram. Soc. Jpn.* **104**, 734 (1996).
5. Murrell, L. L., *Catal. Today* **35**, 225 (1997).
6. Utiyama, M., Hattori, H., and Tanabe, K., *Bull. Chem. Soc. Jpn.* **54**, 2521 (1981).
7. Ishikawa, T., Ohashi, R., Nakabayashi, H., Kakuta, N., Ueno, A., and Furuta, A., *J. Catal.* **134**, 87 (1992).
8. Jaworska-Galas, Z., Mista, W., Wrzyszcz, J., Zawadzki, M., and Machnikowski, J., *J. Catal.* **145**, 450 (1994).
9. Segal, D., "Chemical Synthesis of Advanced Ceramic Materials." Cambridge Univ. Press, Cambridge, 1989.
10. Janosovite, U., Ziegler, G., Scharf, U., and Wokaun, A., *J. Non-Cryst. Solids* **210**, 1 (1997).
11. Machida, M., Eguchi, K., and Arai, H., *Bull. Chem. Soc. Jpn.* **61**, 3659 (1989).
12. Mizushima, Y., and Hori, M., *J. Mater. Res.* **9**, 2272 (1994).
13. Boccaccini, A. R., Trusty, P. A., and Teller, R., *Mater. Lett.* **29**, 171 (1996).
14. Yoldas, B. E., *Amer. Ceram. Soc. Bull.* **54**, 286 (1975).
15. Yoldas, B. E., *J. Mat. Sci.* **10**, 1856 (1975).
16. Pajonk, G. M., *Rev. Chem. Appl.* **24**, 13 (C4) (1989).
17. Murrell, L. L., Dispenziere, N. C., Jr., and Kim, K. S., *ACS Symp. Ser.* **437**, 97 (1990).
18. Murrell, L. L., and Tauster, S. J., *in* "Proc. 2nd Int. Congress on Catalysis and Automotive Pollution Control, CAPoC, Brussels, Belgium, 1990," p. 547.
19. Pajonk, G. M., *Catal. Today* **35**, 319 (1997).
20. Mizushima, Y., Hori, M., and Saaki, M., *J. Mater. Res.* **8**, 2109 (1993).
21. Mizushima, Y., and Hori, M., *J. Non-Cryst. Solids* **167**, 1 (1994).
22. Horiuchi, T., Osaki, T., Sugiyama, R., Masuda, H., Horio, M., Suzuki, K., Mori, T., and Sago, T., *J. Chem. Soc. Farad. Trans.* **90**, 2573 (1994).
23. Ponthieu, E., Payen, E., and Grimblot, J., *in* "Sol-Gel Processing and Applications" (Y. A. Attia, Ed.), p. 221. Plenum, New York, 1994.
24. Khalil, K. M. S., Baird, T., Zaki, M. I., and El-Samahy, A. A., "Electron Microscopy," Vol. 2, p. 421. Eurem 92, Granada, Spain, 1992.
25. Khalil, K. M. S., Ph.D. thesis, Assiut Univ., Sohag, Egypt, 1994.
26. JCPDS, International Center for Diffraction Data, CD, 1996.
27. Brunauer, B., Emmett, P. H., and Teller, E., *J. Am. Chem. Soc.* **60**, 309 (1938).
28. Refer to "Micromertics DFT Plus, Operator's Manual." V1.00, 1996.
29. International Union of Pure and Applied Chemistry, IUPAC, *Pure & Appl. Chem.* **57**, 603 (1985).
30. Brinker, C. J., and Scherer, G. W., *in* "Sol-Gel Science, The Physics and Chemistry of Sol-Gel Processing," p. 78. Academic Press, New York/London, 1989.
31. Assih, T., Ayral, A., Abenoza, M., and Phalippou, J., *J. Mat. Sci.* **23**, 3326 (1988).
32. Dwivedi, R. K., and Gowda, G., *J. Mat. Sci. Lett.* **4**, 331 (1985).
33. Wilson, S. J., and Stacey, M. H., *J. Coll. Int. Sci.* **82**, 507 (1981).
34. Yang, X., Pierre, A. C., and Uhlmann, D. R., *J. Non-Cryst. Solids* **100**, 371 (1988).
35. Pierre, A. C., and Uhlmann, D. R., *J. Non-Cryst. Solids* **82**, 271 (1986).
36. Soled, S., *J. Catal.* **81**, 252 (1983).